# USING ORGANOTYPIC RAFT CULTURES TO UNDERSTAND THE BIOLOGICAL BASIS OF RAMAN SPECTRA FROM SKIN

By

Matthew David Keller

Thesis

Submitted to the Faculty of the

Graduate School of Vanderbilt University

in partial fulfillment of the requirements

of the degree of

MASTER OF SCIENCE

in

Biomedical Engineering

May, 2006

Nashville, Tennessee

Approved:

Professor Anita Mahadevan-Jansen

Professor Frederick R. Haselton

# ACKNOWLEDGMENTS

I would like to thank the Howard Hughes Medical Institute for their financial support in awarding me a pre-doctoral fellowship, and the National Institutes of Health for funding the actual research. I would of course like to acknowledge my advisor, Dr. Anita Mahadevan-Jansen, for her guidance through this research and for understanding when everything did not go according to plan.

Many other people were vital to this research. A big thanks goes to Evelyn Okediji for spending so much time refining the method of processing raft cultures for histology, and to Amy Viehoever and Jerry Wilmink for their help in creating and improving the rafts. Chad Lieber and Matthijs Grimbergen taught me a great deal about our instrumentation, and the Matlab codes that they wrote have saved me a great deal of time over the years.

Finally, I would like to thank my parents for always encouraging me in all my academic ventures, and my beautiful wife Kelly for her support, listening to my frustrations at times, and motivating me to make sure I'm not a student forever.

TABLE OF CONTENTS

LIST OF FIGURES

# CHAPTER I

# INTRODUCTION

## Motivation and objectives

Recent studies in our lab have shown that organotypic raft cultures have Raman spectra closely mimicking those of actual tissue, particularly epithelial tissues like cervix and skin. Other studies in our lab have demonstrated that Raman spectroscopy can discriminate among basal cell carcinoma (BCC), squamous cell carcinoma (SCC), non-normal benign (e.g. scar), and normal skin *in vivo*. Although the neoplasms tend to arise in or invade fairly deeply in the epidermis, the optimal depth of measurement for discrimination purposes is about 40 μm. The primary objective of this work was to determine how the location and concentration of SCC cells within raft cultures affect the Raman spectral signatures of the rafts. Further goals were to investigate the depth dependence of the cancerous cell locations and measurement sites, and to correlate spectroscopic findings with histology.

## Specific aims

The following specific aims were developed to guide my research regarding the objectives stated above:

1. *Modify raft cultures to include SCC cells in the dermis*. Raft cultures were previously always constructed with normal dermis layers and either normal or dysplastic epidermal

layers, so my first task was to figure out how to make rafts with cancerous cells in their stromal layers.

2. *Obtain and compare Raman spectral signatures of rafts with dysplastic cells in their stroma to previous raft constructs*. Raman spectroscopy has previously been used in our lab to examine normal raft cultures and rafts with dysplastic epidermal layers, but spectral signatures from those types needed to be compared with spectral signatures of rafts with dysplastic cells in their stroma.

3. *Determine the depth dependence of the source of Raman spectral discrimination in the earlier* in vivo *study*. The epidermal and stromal layers of the rafts were separated and measured to determine whether distal disease could be detected near the surface.

4. *Compare spectroscopic findings with histology*. Biopsy is still the gold standard of skin cancer diagnosis, so Raman spectral measurements have to be evaluated alongside histological findings of the raft cultures to verify the tissue status.

As a result of these specific aims, we expected to find that raft cultures could still be reliably produced with SCC cells in the dermal layer, and that the spectra of these rafts would at least closely resemble those of rafts with SCC cells in the epidermis and a normal dermis. We believed that stromal disease would be detected in the epidermal layers, with histology showing that layer to still look fairly normal.

# CHAPTER II

# BACKGROUND

Skin cancer is a major problem in the United States that continues to get worse, as the incidence increases by 5-10 % each year. The various major forms of skin cancer: melanoma, basal cell carcinoma (BCC), and squamous cell carcinoma (SCC), account for over half of the cancer cases in the US. The nonmelanoma cancers (BCC and SCC) account for about 95 % of the 1.3 million new cases of skin cancer each year, and BCC comprises the majority of these cases with 75-80 %, while SCC comprises 15-20 % of cases. Although malignant melanoma accounts for only 4 % of new skin cancer cases each year, it is responsible for nearly 80 % of the estimated 10,000 deaths each year from skin cancer.[1]

## Normal Skin Histology

A basic understanding of normal skin histology is essential for further discussion on skin cancer. As seen in Figure 1, skin is typically divided into three layers: the epidermis, dermis, and hypodermis, although this bottom layer is rarely important in skin cancer. The dermis, usually 0.3 to 3 mm thick, is further divided into the papillary and reticular layers as seen in Figure 1.1. The papillary layer consists primarily of small blood vessels and fine collagen and elastic fibers, and the reticular layer contains the larger vascular plexus as well as compact collagen and thick elastic fibers. In both layers, fibroblasts are the primary cell, and they produce much of the extracellular matrix.[2]

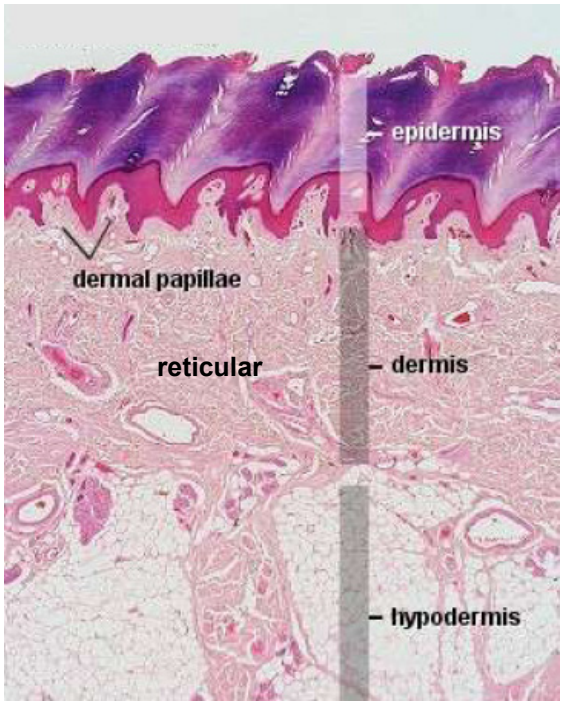


**Figure 1.1** Histology of normal skin[3]

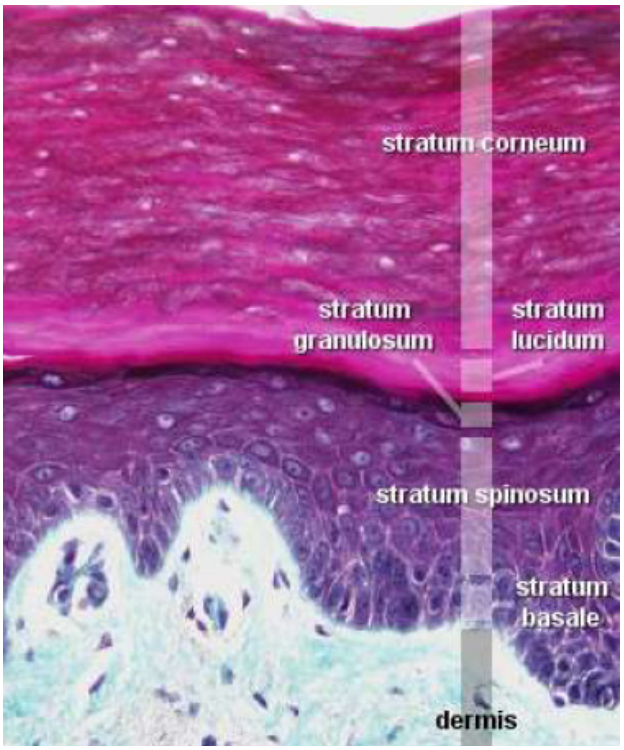


**Figure 1.2** Closer look at the epidermis[3]

The epidermis is usually around 0.1 mm thick, though it can grow to about 1 mm on the palms and soles. It is further divided into five layers: the strata basale (or germinativum), spinosum, granulosum, lucidum, and corneum, going from bottom to top as seen in Figure 1.2. The stratum basale contains the basal cells, or germ cells, that continually divide to replace cells that have undergone keratinization, which is the process of keratinocytes flattening, losing their nuclei, and accumulating keratin before dying to form the water-proof stratum corneum. Keratin filaments, which attach at desmosomes and are crosslinked by fillagrin to form large aggregates, are essential for the structural stability and integrity of the epithelium as the keratinocytes mature and move outward. The stratum basale also contains the pigment-producing melanocytes and sensory Merkel cells. The only other cell type in the epidermis is the Langerhans cell, which is involved in immune functions in the middle layers of the epidermis.[2,4]

The area between the top two skin layers is referred to as the dermoepidermal junction, which consists of the lamina lucida and lamina densa. The lamina lucida is in contact with the epidermis, and it consists of anchoring proteins such as laminin 6, p105, and p200. The thicker lamina densa contacts the dermis and consists primarily of laminin 5 and BP180. Other components typically found in the region include BP240, collagen IV, and $\alpha_6\beta_4$ integrin.[2]

**Basal Cell Carcinoma**

The most common cancer in humans, basal cell carcinoma is defined as a malignant neoplasm derived from nonkeratinizing cells that originate in the basal layer (stratum basale) of the epidermis. BCC can invade and damage surrounding tissues, but

it metastasizes in less than 0.5% of cases. The biggest risk factors for BCC include ultraviolet light exposure, fair skin, Celtic ancestry, an inability to tan, and exposure to ionizing radiation.[2] Development of BCC can take from several months to several years after the initiating event to become clinically presentable. More than 80% of all BCCs occur on the head and neck, though not always in areas of greatest UV exposure, and men and older people are affected more than women and younger people. Over 99% of cases can be cured, but there is a 45% chance for developing another BCC within 3 years, and the 5 year recurrence rate is around 8%.[5]

A number of histologic features define BCC. The cells are basophilic, arise from and resemble basal cells of the epidermis, have increased nucleus to cytoplasm ratios, and lack prominent nucleoli and intercellular bridges. The tumors tend to form nests with basal layers surrounding them, a condition known as palisading, which is shown in Figure 1.3. A mucinous stroma forms around the tumor parenchyma, and the stroma

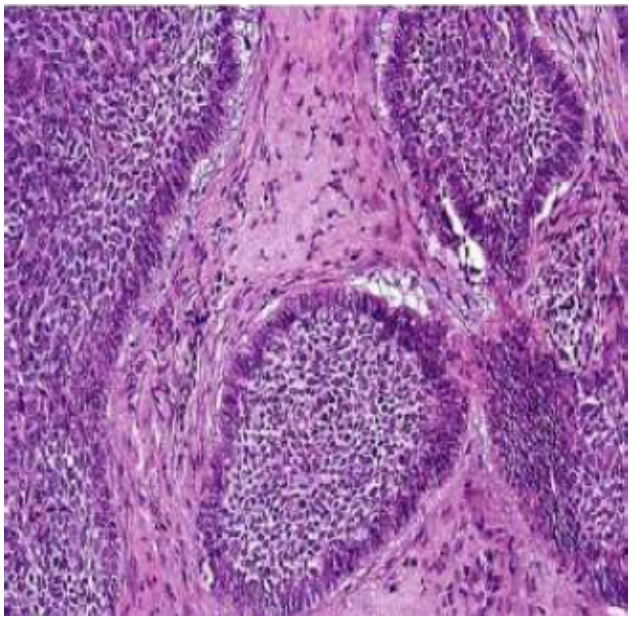

**Figure 1.3** Nodular BCC demonstrating palisading around tumor nests[3]

tends to retract from tumor islands upon examination, creating peritumoral lacunae. A BCC cannot grow well without its stroma, so only the most aggressive tumors can metastasize.[6]

There are five major clinical subtypes of BCC: nodular, pigmented, superficial, morpheaform, and fibroepithelioma of Pinkus. Nodular BCC is the most common form, and it presents as a translucent papule or nodule, often with telangiectasias and a rolled border. Histopathologically, nodular BCC looks like Figure 1.3 with tumor nests and palisading. Pigmented BCC is any BCC with a large amount of melanin, though this typically occurs with nodular BCC. Superficial BCC, as shown in Figure 1.4, consists of tumor cells budding down into the dermis and palisading. It can resemble eczema or

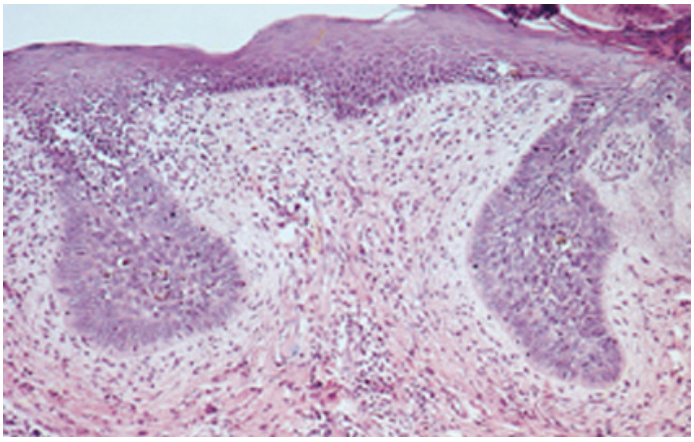

**Figure 1.4** Superficial BCC from cross section[5]

psoriasis, and it is the least aggressive BCC, typically found on the trunk. In contrast to superficial BCC, morpheaform, or infiltrative BCC, is quite aggressive and is likely to recur since it is often larger than it appears on the surface. It consists of tumor cells tightly packed in a dense stroma that can extend deep within the dermis, as shown in

Figure 1.5. Morpheaform BCC often resembles a scar, and it can even develop from an old scar. Fibroepithelioma of Pinkus appears as long strands of interwoven basiloma cells embedded in fibrous stroma.[2,5]

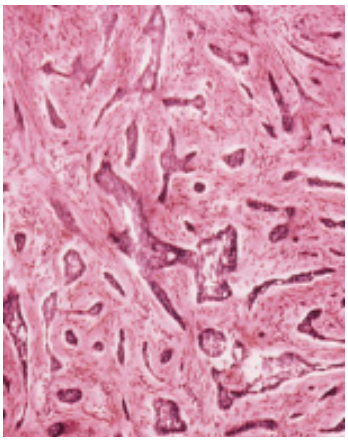

**Figure 1.5** Histology of morpheaform BCC[2]

On a smaller scale, BCC cells express low molecular weight keratin peptides but not high molecular weight ones. In this manner, they resemble both basal epidermal and follicular epithelial cells. The tumor stroma contains the usual laminin and collagen IV, but the BP240 is typically not present around tumor islands. In addition, BCC cells have sparse mitochondria, granular endoplasmic reticula, prominent desmosomes, and abundant tonofilaments.[7]

**Squamous Cell Carcinoma**

SCC is defined as a neoplasm arising from suprabasal keratinocytes in the epidermis, often from the stratum spinosum, and invading downward through the dermis. Although BCC is much more common than SCC, the greater ability of SCC to metastasize (0.5-6% of cases metastasize to regional lymph nodes 1 to 3 years after initial

diagnosis) makes it responsible for most nonmelanoma skin cancer deaths.[5] The incidence of SCC increases drastically with age, and it often develops out of precursor legions such as actinic keratoses and Bowen's disease, or SCC *in situ*. Other primary risk factors include UV and ionizing radiation exposure, fair skin, thermal burns or other scars, certain strains of human papilloma virus, and mutations in the tumor suppressor p53 and apoptosis-inhibitor Bcl-2, inhibiting the former and activating the latter.[2] SCC can be found in highly sun-exposed areas as well as on the scalp and on the back of the hands, two places where BCC is rarely found.[5]

SCC often presents as a firm, flesh-colored or erythematous, keratotic papule or plaque, though pigmentation, ulcer, and a cutaneous horn may also be present. The histopathology of a typical SCC is shown below in Figure 1.6. The defining characteristic is the presence of atypical keratinocytes extending beyond the basement membrane into the dermis, though they can appear as single cells, nests of cells, or a single mass. The atypical cells themselves are characterized by increased mitoses,

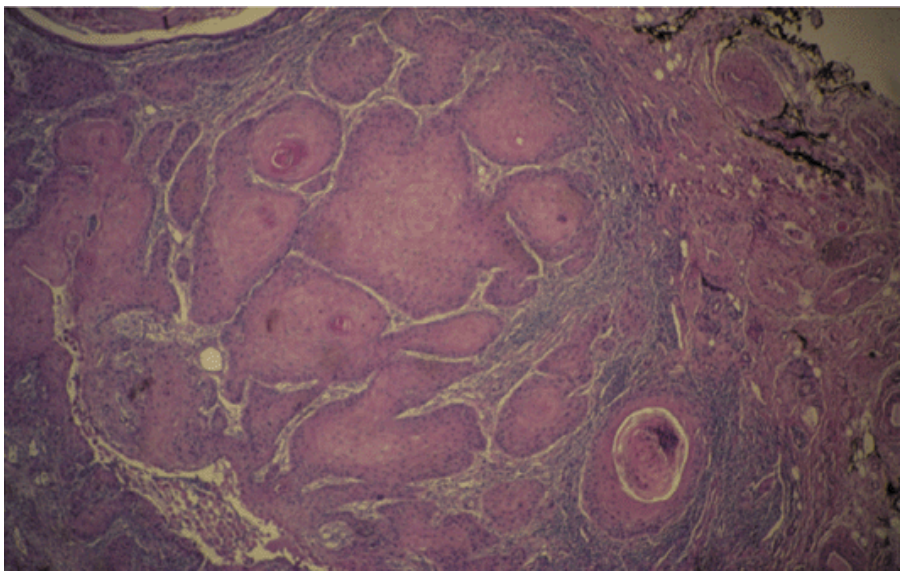

**Figure 1.6** Standard histology section of invasive SCC[2]

aberrant mitotic figures,nuclear hyperchromasia, and loss of intercellular bridges. Grading of the tumor is based on degree of differentiation of the cells, where more aggressive tumors are less differentiated. This dedifferentiation is observed as a reduction in keratin production and loss of intercellular bridges. Other signs of an aggressive tumor include poorly defined margins between the tumor and normal stroma, a size larger than 2 cm, invasion greater than 4 mm deep, and an origin at the lips or in scar tissue. Histologic subtypes of SCC include adenoid, clear cell, spindle cell, signet-ring cell, verrucous carcinoma, and keratocanthoma.[2]

A number of studies have been performed to investigate the biochemical changes in and around SCC.[8-10] Active remodeling of the ECM into a tumor stroma has been indicated as a key step in the invasion process. Fibroblasts migrate toward the solid tumor through an unclearly defined mechanism possibly involving type I collagen expression, where they then differentiate toward becoming myofibroblasts. Poorly differentiated SCCs show diffuse localization of myofibroblasts, whereas more differentiated SCCs show only a local distribution of them. Type I collagen synthesis has shown a very high degree of correlation with invasive SCC tumor fronts, presumably as the body's effort to encapsulate the tumor and prevent further growth. Despite this increase in collagen I synthesis, the tumor stroma of the more aggressive neoplasias actually have a reduced and disordered collagen content.[8] This disorder of the matrix proteins is generally attributed to various collagenases and matrix metalloproteinases (MMPs), especially MMP-2 and MMP-9, that are necessary for the invasion process.[11]

Other studies have examined the role of internal biochemical pathways in SCC. The levels of extracellular $Ca^{2+}$ play a large role in keratinocyte differentiation, so

accordingly protein kinase C (PKC) is a major player in SCC. PKCα, one particular isozyme, has been shown to be responsible for many of the characteristic biochemical changes in SCC, including inhibition of keratin 1 and 10 expression and up-regulation of loricrin, filaggrin, and transglutanimase-1.[9] Other specific biochemical changes in SCC include upregulation of keratins K13, K14, and K19,[10] abnormalities in chromosomes 6 and 7, loss of TGFβ1, and upregulation of $\alpha_6\beta_4$ integrin.[9]

**Current Diagnosis and Treatment**

Diagnosis of a nonmelanoma skin cancer requires a biopsy to be taken and then read by a trained pathologist. For both BCC and SCC, if the lesion is primarily superficial, a shave biopsy may be sufficient; if the lesion appears to involve deeper tissue, then a punch biopsy is required.[12] This method can be slow, subjective, and painful, so a number of non-invasive diagnostic techniques are being investigated. CT and MRI can be used to examine the extent of disease, especially in sensitive areas like the head and neck. MRI is better suited for looking at soft tissue invasion, while CT is better for detecting bone invasion. Ultrasound and nuclear medicine techniques, primarily SPECT and FDG-PET, can also be used to help distinguish inflammation and necrosis from recurrent tumor.[6]

The most common treatment methods for BCC and SCC include electrodessication and curettage (ED&C), cryosurgery, surgical excision, radiation therapy, and Mohs micrographic surgery. The first four are fairly self-explanatory; Mohs micrographic surgery is a more complex process. A thin horizontal section is cut from the entire surface of the gross tumor, stained, and divided into quadrants from which a

map is drawn. The excised pieces are then frozen sectioned and microscopically examined to note the locations of cancer on the map. Deeper horizontal sections are then taken only from quadrants that contained cancerous cells, and this process is repeated until none of the sections shows any signs of cancer, indicating complete removal.[12]

The treatment chosen for BCC depends on the subtype and location of the tumor. ED&C is the treatment of choice for small nodular lesions on the face and any tumors on the trunk or extremities, and surgical excision can be used on these as well but is more often reserved for recurrent cases. Cryotherapy is generally limited to superficial tumors on the trunk, and radiation therapy is reserved for inoperable tumors. Mohs micrographic surgery is used for any tumors in sensitive areas of the face and can be used for recurrent cases elsewhere.[12]

Treatment protocols for SCC are similar to those for BCC but have some differences. ED&C is typically used for SCC *in situ* and other superficial cases, and surgical excision is used for other accessible primary lesions. Cryosurgery is generally limited to treating pre-cancerous lesions, and radiation therapy is again used only for inoperable cases. Mohs micrographic surgery is used as it is for BCC and for other aggressive tumors. Alternative treatments sometimes applied to SCC include $CO_2$ laser excision, photodynamic therapy, and topical application of the chemotherapeutic 5-fluorouracil on pre-cancerous lesions only.[12]

**Optical spectroscopy**

There are drawbacks to current diagnostic methods for skin cancer. They rely on initial visual inspection, which can be error-prone (especially with regard to false

positives), and tissue biopsy, which is a subjective, relatively costly, and slow procedure. Biopsy can also be more painful than the actual treatment procedure. There is thus a need for an accurate, real-time, non-invasive diagnostic tool. Various methods of optical spectroscopy have been used in attempts to achieve this goal, particularly fluorescence, elastic scattering, and Raman spectroscopy.

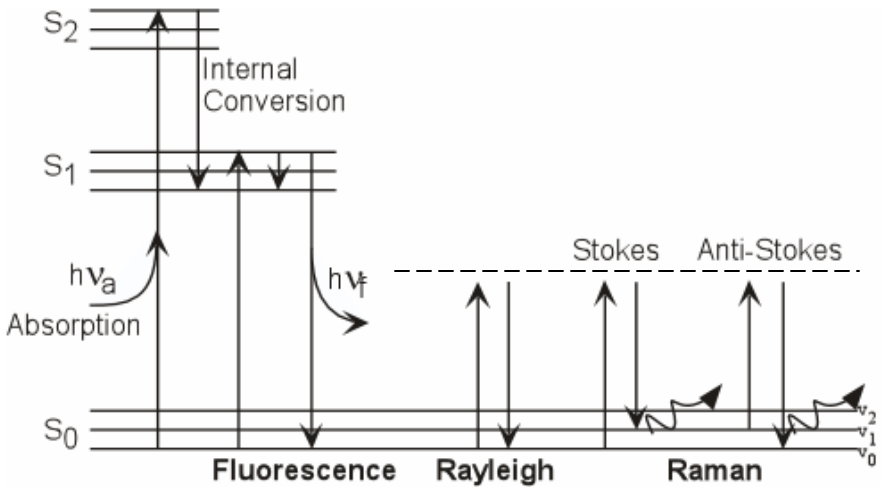


**Figure 1.7** Jablonski diagram illustrating physical principles of common optical spectroscopic modalities. $S_i$ refers to electronic energy levels; $v_i$ to vibrational ones. Dashed line represents a virtual excited state.

*Fluorescence and diffuse reflectance*

As shown in Figure 1.7, fluorescence involves absorption of a photon, internal conversion (heat dissipation), and then re-release of a photon of lower energy. In tissue, autofluorescence signals from certain compounds like NADH, collagen, and flavins provide information about the metabolic or biochemical status of the tissue, and can thus distinguish between healthy and diseased states. Elastic, or Rayleigh, scattering involves an incident photon getting its path changed without losing or gaining any energy. This

technique, also known as diffuse reflectance, provides morphological information about the tissue, such as number and size of scattering nuclei. Since these two techniques both have strong signals and provide complementary information, they are often combined to maximize diagnostic potential. Fluorescence and diffuse reflectance have been applied to cancer detection in many areas of the body, including cervix,[13-15] skin,[16, 17] breast,[18-20] and brain.[21, 22] While these techniques have experienced success in certain areas, the broad peaks can limit their ability to distinguish among many different classes of disease,[23] and especially in skin, pigmentation and external chemicals can severely limit the penetration depth of the UV excitation source.

*Raman spectroscopy*

Raman spectroscopy utilizes its namesake inelastic scattering, which occurs when an incident photon causes a scattering molecule to enter a virtual excited state, and then return to a ground state either higher or lower than the original through the emission of another photon, as seen on the right side of Figure 1.7. Raman Stokes scattering occurs when the scattered photon has less energy than the incident photon, while Raman Anti-Stokes scattering occurs when the scattered photon has more energy than the incident photon. In contrast to fluorescence, which involves transitions between electronic energy levels, Raman scattering exploits smaller transitions between vibrational energy levels. This less intense signal requires a powerful laser source and a sensitive detector, and the much stronger fluorescence must be subtracted from the raw spectrum as well.

A Raman spectrum is a plot of scattered light intensity versus the frequency shift of the scattered photon, making it independent of excitation wavelength. The frequency

shift is expressed in units of wavenumber, which is the reciprocal of the wavelength, so it is proportional to frequency. The spectrum consists of a series of peaks, each of which represents a different vibrational mode of the scattering molecule. These peaks are narrow and highly specific to a particular chemical bond, so each molecule has a unique spectrum, or "fingerprint," associated with it from about 700 to 2000 $cm^{-1}$. Many biological molecules have distinguishable spectra, so one can determine the gross biochemical composition of a tissue from its Raman spectrum. One particularly relevant biochemical change previously discussed for cancer cells is an increase in the nucleic acid content concomitant with increased proliferation and genetic instability. This change, among others, can be detected with Raman spectroscopy.[24, 25]

Raman spectroscopy was historically used in analytical chemistry to determine chemical structures or the presence of certain molecules, and it has only been in the last ten or twelve years that it has become a more popular choice for studying tissue. The majority of studies have been *in vitro*, attempting to distinguish normal from cancerous tissue in areas like cervix[26], breast,[27-29] bladder and prostate,[27,30] lung,[31] and the GI tract.[27] Many have written of the challenges of bringing Raman to *in vivo* applications,[32, 33] but it has been successfully applied to cervix,[34] GI tract,[35, 36] and breast.[37]

Human skin, because of its ease of access, has seen a great deal of study by Raman spectroscopy. Earlier *in vitro* studies used mostly FT-Raman to examine skin structure[38-43] and to attempt to distinguish normal from cancerous tissues.[44, 45] The instrumentation for FT-Raman prevents its use in a clinical setting, so a more recent *in vitro* study used traditional Raman spectroscopy to distinguish BCC from normal tissue by producing two-dimensional Raman images.[46] Many *in vivo* studies have been

performed as well, especially examining carotenoid content of the skin,[47-50] which is thought to play a role in defense against malignancy. Other fiber probe-based *in vivo* studies have investigated various structural and biochemical aspects of the skin,[51-54] and several groups have used Raman spectra in combination with fluorescence or advanced multivariate statistical techniques to enhance discrimination between normal and cancerous tissues.[55-57]

Since the skin is a stratified tissue, a major goal for dermatological applications is having depth-resolved data. To this end, several groups have applied confocal Raman spectroscopy or Raman microspectroscopy to gather data from only a thin layer of the skin at a time. These techniques have been applied *in vivo* both to determining molecular concentration profiles[58-60] and to discriminating between normal skin and BCC.[61] In our lab, a previous study used confocal Raman spectroscopy to distinguish among SCC, BCC, and non-normal benign tissues (e.g. scar) when comparing the spectra to their respective normal spectra.[62]

**References**


1. American Cancer Society. www.cancer.org. (2005).

2. Freedberg I *et. al., eds.* Fitzpatrick's Dermatology in General Medicine, 6th edn. (McGraw Hill: 2003).

3. http://fisica.ist.utl.pt/~left/2003-2004/Apresentacoes/TeresaCorreia.pdf. (2005).

4. Young B, Heath J, eds. Wheater's Functional Histology, 4th edn. (Churchill Livingstone: 2005).

5. Habif T. Clinical Dermatology: A Color Guide to Diagnosis and Therapy, 4th edn. (Mosby, New York: 2004).

6. Weber R, Miller M, Goepfert H, eds. Basal and Squamous Cell Skin Cancers of the Head and Neck. (Williams & Wilkins, Baltimore: 1996).

7. Friedman R *et. al., eds.* Cancer of the Skin. (WB Saunders Company, New York: 1991).

8. van Kempen L, Rijntes J, Claes A, Blokx W, Gemtsen M, Ruiter D, van Muijen G. Type I collagen synthesis parallels the conversion of keratinocytic intraepidermal neoplasia to cutaneous squamous cell carcinoma. *J Pathol* **204**, 333-339 (2004).

9. Yuspa S. The pathogenesis of squamous cell cancer: lessons learned from studies of skin carcinogenesis. *J Dermatol Sci*. **17**(1),1-7 (1998).

10. Yuspa S, Lee P, Hennings H, Strickland J, Cheng C, Glick A, Dlugosz A. The in vitro analysis of biochemical changes relevant to skin carcinogenesis. *Recent Results Cancer Res*. **128**, 299-308 (1993).

11. Kerkelä E, Saarialho-Kere U. Matrix metalloproteinases in tumor progression: focus on basal and squamous cell skin cancer. *Experimental Dermatology* **12**, 109–125 (2003).

12. Moy R, Taheri D, Ostad A. Practical Management of Skin Cancer. (Lippincott-Raven, Philadelphia: 1999).

13. Mitchell, M.F., Cantor, S.B., Ramanujam, N., Tortolero-Luna, G. & Richards-Kortum, R. Fluorescence spectroscopy for diagnosis of squamous intraepithelial lesions of the cervix. *Obstet Gynecol* **93**, 462-470 (1999).

14. Ramanujam, N. Fluorescence spectroscopy of neoplastic and non-neoplastic tissues. *Neoplasia* **2**, 89-117 (2000).

15. Ramanujam, N. et al. Spectroscopic diagnosis of cervical intraepithelial neoplasia (CIN) in vivo using laser-induced fluorescence spectra at multiple excitation wavelengths. *Lasers Surg Med* **19**, 63-74 (1996).

16. Brancaleon, L. et al. In vivo fluorescence spectroscopy of nonmelanoma skin cancer. *Photochem Photobiol* **73**, 178-183 (2001).

17. Gillies, R., Zonios, G., Anderson, R.R. & Kollias, N. Fluorescence excitation spectroscopy provides information about human skin in vivo. *J Invest Dermatol* **115**, 704-707 (2000).

18. Breslin, T.M. et al. Autofluorescence and diffuse reflectance properties of malignant and benign breast tissues. *Ann Surg Oncol* **11**, 65-70 (2004).

19. Gupta, P.K., Majumder, S.K. & Uppal, A. Breast cancer diagnosis using N2 laser excited autofluorescence spectroscopy. *Lasers Surg Med* **21**, 417-422 (1997).

20. Palmer, G.M., Keely, P.J., Breslin, T.M. & Ramanujam, N. Autofluorescence spectroscopy of normal and malignant human breast cell lines. *Photochem Photobiol* **78**, 462-469 (2003).

21. Lin, W.C., Toms, S.A., Johnson, M., Jansen, E.D. & Mahadevan-Jansen, A. In vivo brain tumor demarcation using optical spectroscopy. *Photochem Photobiol* **73**, 396-402 (2001).

22. Lin, W.C., Toms, S.A., Motamedi, M., Jansen, E.D. & Mahadevan-Jansen, A. Brain tumor demarcation using optical spectroscopy; an in vitro study. *J Biomed Opt* **5**, 214-220 (2000).

23. Ramanujam, N. et al. Development of a multivariate statistical algorithm to analyze human cervical tissue fluorescence spectra acquired in vivo. *Lasers Surg Med* **19**, 46-62 (1996).

24. Mahadevan-Jansen, A. in Biomedical Photonics Handbook. (ed. T. Vo-Dinh) (CRC Press, Washington DC; 2003).

25. Mahadevan-Jansen, A., Richards-Kortum, R. Raman Spectroscopy for the Detection of Cancers and Precancers. *J Biomed Optics* **1**, 31-70 (1996).

26. Mahadevan-Jansen, A. et al. Near-infrared Raman spectroscopy for in vitro detection of cervical precancers. *Photochem Photobiol* **68**, 123-132 (1998).

27. Frank, C.J., McCreery, R.L. & Redd, D.C. Raman spectroscopy of normal and diseased human breast tissues. *Anal Chem* **67**, 777-783 (1995).

28. Stone, N., Kendall, C., Smith, J., Crow, P. & Barr, H. Raman spectroscopy for identification of epithelial cancers. *Faraday Discuss* **126**, 141-157; discussion 169-183 (2004).

29. Haka, A.S. et al. Identifying microcalcifications in benign and malignant breast lesions by probing differences in their chemical composition using Raman spectroscopy. *Cancer Res* **62**, 5375-5380 (2002).

30. Crow, P. et al. Assessment of fiberoptic near-infrared raman spectroscopy for diagnosis of bladder and prostate cancer. *Urology* **65**, 1126-1130 (2005).

31. Huang, Z. et al. Near-infrared Raman spectroscopy for optical diagnosis of lung cancer. *Int J Cancer* **107**, 1047-1052 (2003).

32. Choo-Smith, L.P. et al. Medical applications of Raman spectroscopy: from proof of principle to clinical implementation. *Biopolymers* **67**, 1-9 (2002).

33. Hanlon, E.B. et al. Prospects for in vivo Raman spectroscopy. *Phys Med Biol* **45**, R1-59 (2000).

34. Mahadevan-Jansen, A., Mitchell, M.F., Ramanujam, N., Utzinger, U. & Richards-Kortum, R. Development of a fiber optic probe to measure NIR Raman spectra of cervical tissue in vivo. *Photochem Photobiol* **68**, 427-431 (1998).

35. Shim, M.G., Song, L.M., Marcon, N.E. & Wilson, B.C. In vivo near-infrared Raman spectroscopy: demonstration of feasibility during clinical gastrointestinal endoscopy. *Photochem Photobiol* **72**, 146-150 (2000).

36. Molckovsky, A., Song, L.M., Shim, M.G., Marcon, N.E. & Wilson, B.C. Diagnostic potential of near-infrared Raman spectroscopy in the colon: differentiating adenomatous from hyperplastic polyps. *Gastrointest Endosc* **57**, 396-402 (2003).

37. Haka, A.S. et al. In vivo margin assessment during partial mastectomy breast surgery using raman spectroscopy. *Cancer Res* **66**, 3317-3322 (2006).

38. Edwards, H.G.M., A.C. Williams, and B.W. Barry Potential applications of FT-Raman spectroscopy for dermatological diagnostics. *J Molec Struct* **347**, 379-388 (1995).

39. Neubert, R., Rettig, W., Wartewig, S., Wegener, M. & Wienhold, A. Structure of stratum corneum lipids characterized by FT-Raman spectroscopy and DSC. II. Mixtures of ceramides and saturated fatty acids. *Chem Phys Lipids* **89**, 3-14 (1997).

40. Edwards, C. Raman spectroscopy and skin. *Curr Probl Dermatol* **26**, 20-26 (1998).

41. Caspers, P.J., Lucassen, G.W., Wolthuis, R., Bruining, H.A. & Puppels, G.J. In vitro and in vivo Raman spectroscopy of human skin. *Biospectroscopy* **4**, S31-39 (1998).

42. Osada, M., Gniadecka, M. & Wulf, H.C. Near-infrared Fourier transform Raman spectroscopic analysis of proteins, water and lipids in intact normal stratum corneum and psoriasis scales. *Exp Dermatol* **13**, 391-395 (2004).

43. Gniadecka, M., Faurskov Nielsen, O., Christensen, D.H. & Wulf, H.C. Structure of water, proteins, and lipids in intact human skin, hair, and nail. *J Invest Dermatol* **110**, 393-398 (1998).

44. M. Gniadecka, H.C.W., N. Nymark Mortensen, O. Faurskov Nielsen, D. H. Christensen, Diagnosis of Basal Cell Carcinoma by Raman Spectroscopy. *Journal of Raman Spectroscopy* **28**, 125-129 (1997).

45. Gniadecka, M., Wulf, H.C., Nielsen, O.F., Christensen, D.H. & Hercogova, J. Distinctive molecular abnormalities in benign and malignant skin lesions: studies by Raman spectroscopy. *Photochem Photobiol* **66**, 418-423 (1997).

46. Nijssen, A. et al. Discriminating basal cell carcinoma from its surrounding tissue by Raman spectroscopy. *J Invest Dermatol* **119**, 64-69 (2002).

47. Ermakov, I.V., Sharifzadeh, M., Ermakova, M. & Gellermann, W. Resonance Raman detection of carotenoid antioxidants in living human tissue. *J Biomed Opt* **10**, 064028 (2005).

48. Ermakov, I.V., Ermakova, M.R., Gellermann, W. & Lademann, J. Noninvasive selective detection of lycopene and beta-carotene in human skin using Raman spectroscopy. *J Biomed Opt* **9**, 332-338 (2004).

49. Kollias, N. & Stamatas, G.N. Optical Non-Invasive Approaches to Diagnosis of Skin Diseases. *J Invest Dermat SP* **7**, 64-75 (2002).

50. Hata, T.R. et al. Non-invasive raman spectroscopic detection of carotenoids in human skin. *J Invest Dermatol* **115**, 441-448 (2000).

51. Eikje, N.S., Ozaki, Y., Aizawa, K. & Arase, S. Fiber optic near-infrared Raman spectroscopy for clinical noninvasive determination of water content in diseased skin and assessment of cutaneous edema. *J Biomed Opt* **10**, 14013 (2005).

52. Huang, Z. et al. Raman spectroscopy of in vivo cutaneous melanin. *J Biomed Opt* **9**, 1198-1205 (2004).

53. Z. Huang, H.Z., I. Hamzavi, D. I. McLean, and H. Lui Rapid near-infrared Raman spectroscopy system for real-time in vivo skin measurements. *Opt Lett* **26**, 1782-1784 (2001).

54. Wohlrab, J., Vollmann, A., Wartewig, S., Marsch, W.C. & Neubert, R. Noninvasive characterization of human stratum corneum of undiseased skin of patients with atopic dermatitis and psoriasis as studied by Fourier transform Raman spectroscopy. *Biopolymers* **62**, 141-146 (2001).

55. Huang, Z., Lui, H., McLean, D.I., Korbelik, M. & Zeng, H. Raman spectroscopy in combination with background near-infrared autofluorescence enhances the in vivo assessment of malignant tissues. *Photochem Photobiol* **81**, 1219-1226 (2005).

56. Sigurdsson, S. et al. Detection of skin cancer by classification of Raman spectra. *IEEE Trans Biomed Eng* **51**, 1784-1793 (2004).

57. Gniadecka, M. et al. Melanoma diagnosis by Raman spectroscopy and neural networks: structure alterations in proteins and lipids in intact cancer tissue. *J Invest Dermatol* **122**, 443-449 (2004).

58. Chrit, L. et al. In vivo chemical investigation of human skin using a confocal Raman fiber optic microprobe. *J Biomed Opt* **10**, 44007 (2005).

59. Caspers, P.J., Lucassen, G.W. & Puppels, G.J. Combined in vivo confocal Raman spectroscopy and confocal microscopy of human skin. *Biophys J* **85**, 572-580 (2003).

60. Caspers, P.J., Lucassen, G.W., Carter, E.A., Bruining, H.A. & Puppels, G.J. In vivo confocal Raman microspectroscopy of the skin: noninvasive determination of molecular concentration profiles. *J Invest Dermatol* **116**, 434-442 (2001).

61. Choi, J. et al. Direct observation of spectral differences between normal and basal cell carcinoma (BCC) tissues using confocal Raman microscopy. *Biopolymers* **77**, 264-272 (2005).

62. Lieber, C.A., Ellis, D., Billheimer, D., Mahadevan-Jansen, A. In vivo confocal Raman spectroscopy of skin nonmelanomas. *submitted* (2005).

CHAPTER III

# USING ORGANOTYPIC RAFT CULTURES TO UNDERSTAND THE BIOLOGICAL BASIS OF RAMAN SPECTRA OBTAINED FROM SKIN


## Abstract

Recent studies have shown that organotypic raft cultures have Raman spectra closely mimicking those of actual tissue, particularly epithelial tissues like cervix and skin. Other studies in our lab have demonstrated that Raman spectroscopy can discriminate amongst basal cell carcinoma (BCC), squamous cell carcinoma (SCC), non-normal benign, and normal skin *in vivo*. Although these neoplasms tend to arise in or invade fairly deeply in the epidermis, the optimal depth of measurement in that study for discrimination purposes was about 40 μm. The primary purpose of this work was to determine how the depth and concentration of SCC cells within raft cultures affect the Raman spectral signatures of the rafts. In this manner, raft cultures proved to be useful models in elucidating the biological basis of Raman spectra obtained *in vivo* by controlling where cancerous cells were found within the model during measurements. Raft cultures were constructed with a range of concentrations of SCC cells in the stroma (0.2x to 1x relative to fibroblast concentration) and in the epidermis, and measurements were taken at multiple time points with a macroscopic Raman probe system. The spectra collected with the probe system successfully differentiated normal from cancerous rafts, and they showed that the location and concentration of SCC cells did not have a significant effect on the spectral signatures. In addition, data gathered from the separated epidermal vs. stromal layers, combined with histology, support the hypothesis that

Raman spectroscopy can detect biochemical changes associated with malignancy before such changes are evident via histology.

**Introduction**

Skin cancer is a major problem in the United States that continues to get worse, as the incidence increases by 5-10 % each year. The various major forms of skin cancer: melanoma, basal cell carcinoma (BCC), and squamous cell carcinoma (SCC), account for over half of the cancer cases in the US. The nonmelanoma cancers account for over 95 % of the 1.3 million new cases of skin cancer each year, and BCC comprises the majority of these cases with 75-80 %, while SCC comprises 15-20 % of cases. Although malignant melanoma accounts for only 4 % of new skin cancer cases each year, it is responsible for nearly 80 % of the estimated 10,000 deaths each year from skin cancer.[1] BCC arises from the basal layer of the epidermis, about 100 μm to 1 mm below the surface of skin, so the cells are non-keratinizing and remain relatively undifferentiated. It can invade and damage surrounding tissue, but it very rarely metastasizes. SCC arises from suprabasal keratinocytes, often in the stratum spinosum of the epidermis. It tends to invade downward, and it will occasionally metastasize.[2]

Current diagnostic methods for skin cancer rely on initial visual inspection, which can be error-prone (especially with regard to false positives), and tissue biopsy, which is a subjective, relatively costly, and slow procedure. Biopsy can also be more painful than the actual treatment procedure. There is thus a need for an accurate, real-time, non-invasive diagnostic tool. Given the accessibility of the skin, several modalities of optical spectroscopy have been used in efforts to achieve this goal, but Raman spectroscopy has

seen the most success. Many earlier studies confirmed the ability of Raman to determine molecular composition profiles,[3-5] structures of skin components,[6-9] and water content of the skin[10]. Knudsen *et. al* showed that Raman spectra of skin are reproducible for the most part both within and between patients.[11] The roles of carotenoids[12-14] and lipids[15-18] in skin disease have been investigated with Raman as well. Several papers have reported the ability to distinguish BCC from normal tissue with great success,[19-21] but only limited attempts have been made to discriminate among more than two classes of skin disorders, with varying degrees of success.[22, 23]

Recognizing the need for multi-class discrimination, our recent *in vivo* experiments[24] have demonstrated the ability of Raman spectroscopy to differentiate among normal, non-normal benign (e.g. scar tissue), BCC, and SCC tissues in human skin. The non-melanoma skin cancers arise from fairly deep within the epidermis and tend to invade downward, but the most useful depth of measurement in these experiments turned out to be 40 μm below the surface, which is usually in the middle of the epidermis. One possible explanation for these findings is the presence of so-called malignancy associated changes (MACs), which refer to biochemical changes, such as chromatin rearrangement, in visually normal cells in the vicinity of a tumor that can be detected with ultra sensitive techniques like high resolution cytometry. This idea was first proposed over 40 years ago,[25-27] and more recent studies of tissues such as lung,[28-30] cervix,[31-33] and breast[34-36] have supported the idea. Additionally, Roy *et. al.* have shown the ability of enhanced elastic scattering spectroscopy to detect pre-malignant changes in colon tissue of rats, mice, and humans.[37, 38] Since the true mechanism underlying Raman classification of skin types in our study is not known, though, there is a need to discover

the natures and locations of the sources of the spectral variations that allow discrimination.

Organotypic raft cultures are *in vitro* tissue models of the human skin containing collagen and fibroblasts to model the dermis (stroma) and layers of differentiated keratinocytes to model the epidermis. The Raman spectra of these raft cultures have been shown to replicate the spectra of normal epithelial tissues quite faithfully, and the spectra of raft cultures with cancerous cells replacing keratinocytes also correspond to spectra of cancerous tissue samples. In these raft studies, the majority of the useful spectral variation came from the epidermal layers.[39] The primary purpose of this *in vitro* study was to determine how the location and concentration of SCC cells within raft cultures affect the Raman spectral signatures of the rafts, both macroscopically and within individual layers. Normal rafts, rafts with SCC cells in the epidermis and a normal stroma, and rafts with SCC cells in the stroma and a normal epidermis were constructed, and Raman spectra were obtained at multiple time points of the intact rafts and of the separated epidermis and dermis layers. Raft cultures were processed for histology as well to provide morphological information.

## Materials and Methods

### *Raft culture construction*

Normal raft cultures and rafts with SCC cells (human epidermoid squamous cell carcinoma, A-431) in the epidermis layer only were constructed as described in reference 39. Briefly, normal human dermal fibroblasts (NHDF) were mixed with a concentrated

collagen solution, reconstitution buffer, and concentrated high-glucose Dulbecco's Modified Eagle's Medium (DMEM) in 24 well plates to form the stromal layer. This mixture was incubated at 37 degrees Celsius in 5 % $CO_2$ and 95 % humidity for 24 hours, after which normal human epidermal keratinocytes (NHEK) or SCC cells were added to form the epidermal layer. The rafts were incubated for another 24 hours, and if they had not contracted away from the edge of their plate wells at this time, a thin spatula was run around the edge to aid in contraction. They were incubated for another 24 hours and then placed on metal grids in 60 mm petri dishes. A 50/50 mixture of DMEM and the appropriate media for the epidermal cells was used to feed rafts from below only, and this media was changed every other day. For rafts with SCC cells in the stroma layer, SCC cells were mixed with normal fibroblasts at varying concentrations while keeping the total number of cells in the stroma constant. Only normal keratinocytes were used in the epidermal layer as for normal rafts. In the initial study, the concentrations of SCC cells relative to normal fibroblasts in the stroma for dysplastic rafts were 1x, .6x, .4x, and .2x. Based on initial studies, in subsequent studies SCC cell to NHDF ratios of 1x and .5x, were used. Two to four rafts of each SCC cell concentration were made for each experiment, and four normal rafts were constructed as controls each time.

*Raman measurements*

Raman spectral measurements were obtained as described in reference 39 using the probe system shown below in Figure 2.1, but with an integration time of five seconds. The system consists of a 785 nm diode laser outputting 80 mW at the sample, coupled to a single 400 μm excitation fiber. A bandpass filter at the probe tip cleans up the laser

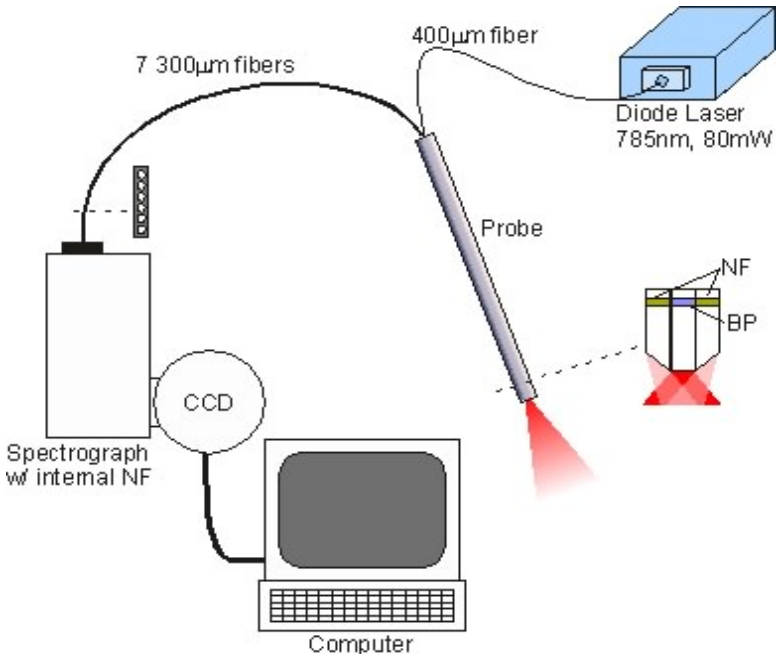


**Figure 2.1** Probe system used to gather Raman spectra. NF, notch filter at 785nm; BP, bandpass filter at 785 nm; CCD, charge-coupled device

light entering the sample, and seven 300 µm fibers collect the backscattered Raman signal, with notch filters at 785 nm to block elastically scattered photons or specularly reflected laser light. The collection fibers then run to a spectrograph to separate the collected light by wavelength and a CCD to capture the spectra. The CCD is connected to a computer to control its operations and record the gathered spectra. Raman measurements were taken at multiple time points as well – at 5, 12, 19, and 26 days following the transfer to the air-liquid interface in the initial study, and at 15 and 20 days for subsequent studies (10 day measurements were initially done as well but eventually dropped). Two measurements were taken from each raft at different locations. After the last time point, one or two rafts of each type were fixed in 10% formalin for histological processing, and the remaining rafts had their epidermal and stromal layers separated and measured as previously described.

*Data processing and analysis*

Collected Raman spectra were processed as in reference 39. In brief, this involved calibrating the wavenumber axis with measurements of neon-argon lamp, acetaminophen, and naphthalene standards, binning the wavenumber axis to 3.5 $cm^{-1}$, and smoothing the data with a second order Savitzky-Golay filter. The background fluorescence was removed with a modified fifth-order polynomial fit, and spectra were normalized to their overall mean intensity to account for any fluctuations in overall intensity. All normalized spectra from each kind of raft at each time point were averaged, and these means were compared at each wavenumber with simple one-way ANOVA and/or a series of 2-sample t-tests. More complicated techniques often used with Raman spectra were deemed unnecessary since we are not trying to develop a discrimination algorithm, but rather we are examining the spectra for qualitative and simple, significant quantitative differences. The spectra for each kind of raft were also averaged over all the time points for a particular study or over multiple studies and examined in a similar fashion.

**Results**

Figure 2.2 below shows the means of all spectra taken in the initial study, which featured only normal rafts and rafts with SCC cells in the stroma layer at varying concentrations. The signal below 1000 $cm^{-1}$ is not shown due to the presence of silica peaks from the fiber optics obscuring any useful biological peaks. A simple visual inspection targeted the area from about 1300 to 1350 $cm^{-1}$ as an area of possible discrimination between normal and dysplastic rafts. A series of t-tests comparing the

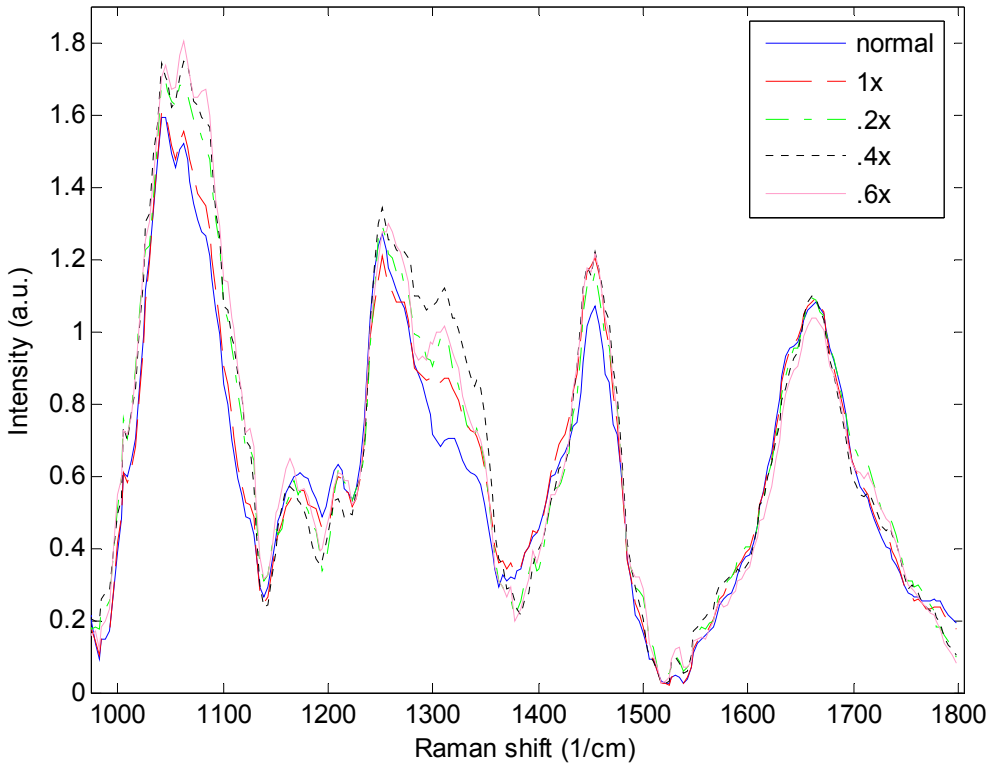


**Figure 2.2** Mean Raman spectra for all time points of initial study for normal rafts (n=18 measurements), and dysplastic rafts with SCC cells at concentrations of 1x (n=18), .2x (n=6), .4x (n=6), and .6x (n=6) relative to that of NHDF cells.

normal rafts with each set of dysplastic rafts at each wavenumber confirmed this observation, giving a significant result at the 0.005 significance level for each comparison over the 1305 to 1330 $cm^{-1}$ range, and nowhere else. It is unclear from the figure whether there is a SCC cell concentration-dependent effect on the signal. No single concentration tested significantly different from all the other concentrations in a series of t tests at any wavenumber, so we concluded that if such an effect exists, it is not significant.

For individual time points of the initial study, day 5 showed little differentiation among the different kinds of rafts. Days 12 and 26 showed a visual, but not statistically significant, discrimination. Figure 2.3 shows the spectra obtained at day 19, which again shows a visual distinction between the normal and dysplastic rafts around 1300 to 1350

$cm^{-1}$. From a series of t-tests at the .01 significance level, the peak at 1450 $cm^{-1}$ is significantly different between normal and dysplastic rafts, as is the shoulder region from 1304 to 1320 $cm^{-1}$. At the .005 significance level, only the minor peak around 1307 – 1310 $cm^{-1}$ remains significantly different between normal and dysplastic rafts. In this case, a visual inspection is enough to conclude that no concentration-dependent effect on the signal is present.

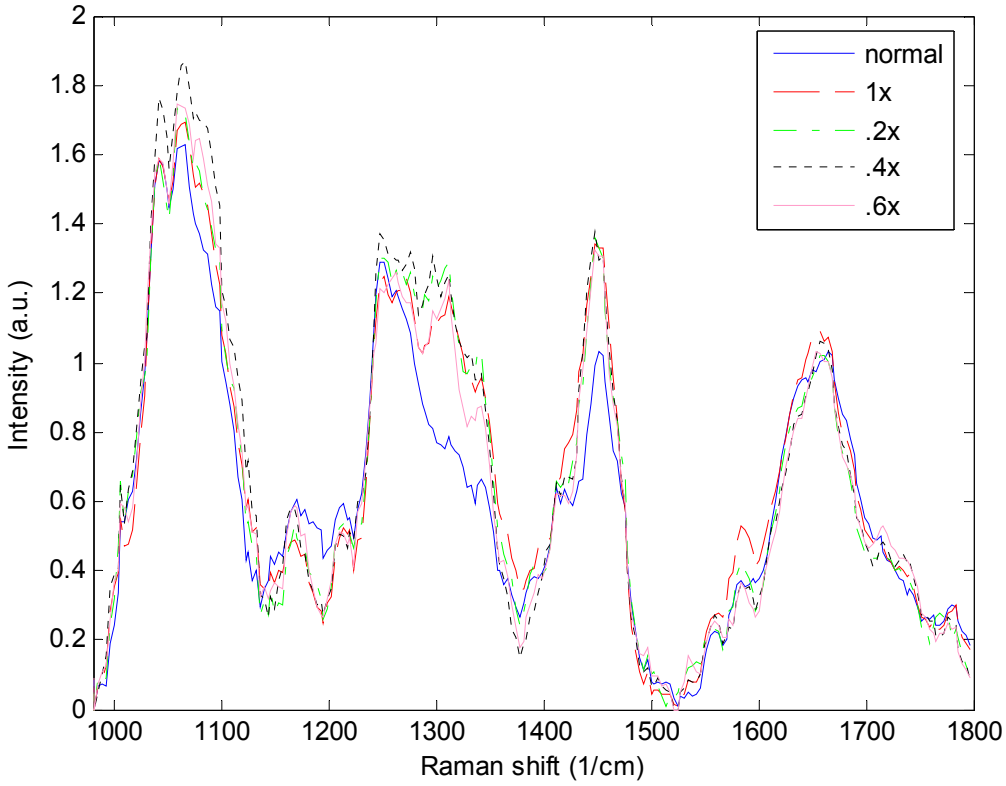


**Figure 2.3** Mean Raman spectra for day 19 of initial study for normal rafts (n=4 measurements), and dysplastic rafts with SCC cells at concentrations of 1x (n=4), .2x (n=2), .4x (n=2), and .6x (n=2).

Based on the results above, a more standardized procedure was developed and used for the remainder of the studies. Figure 2.4 shows the progression of Raman spectra obtained during a single series of experiments at days 10, 15, and 20 following the

**(A)**

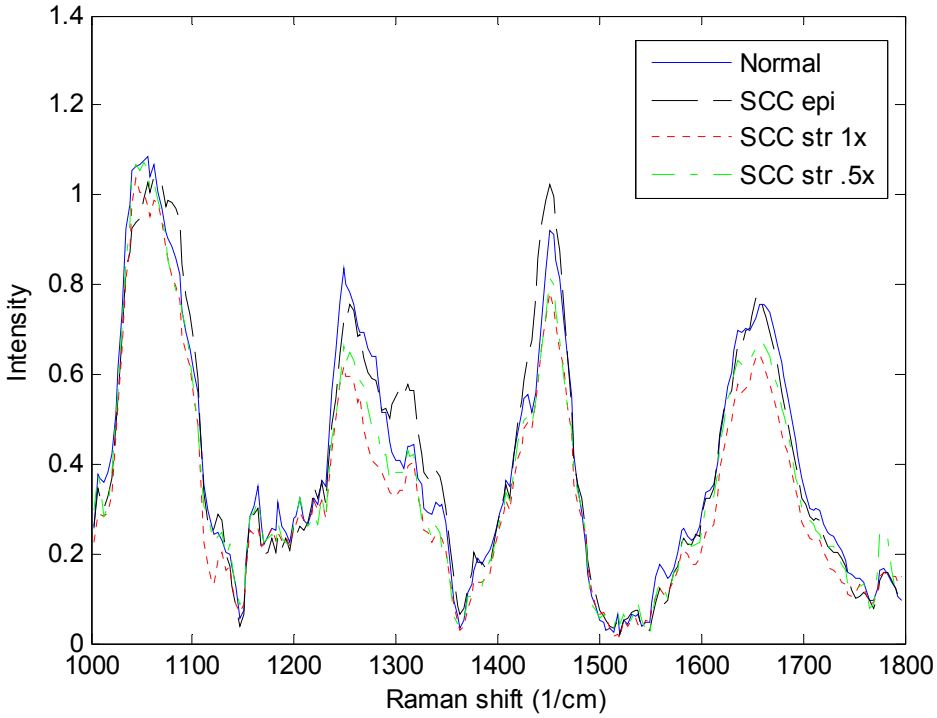
Normal
SCC epi
SCC str 1x
SCC str .5x
Intensity
Raman shift (1/cm)
0
0.2
0.4
0.6
0.8
1
1.2
1.4
1000
1100
1200
1300
1400
1500
1600
1700
1800

**(B)**

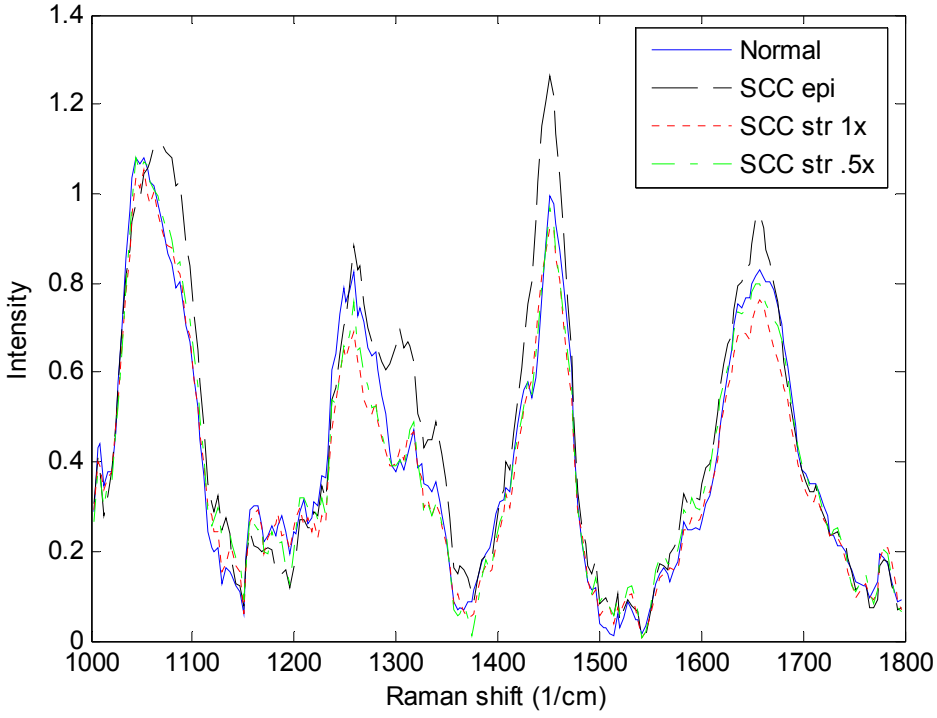
Normal
SCC epi
SCC str 1x
SCC str .5x
Intensity
Raman shift (1/cm)
0
0.2
0.4
0.6
0.8
1
1.2
1.4
1000
1100
1200
1300
1400
1500
1600
1700
1800

**(C)**

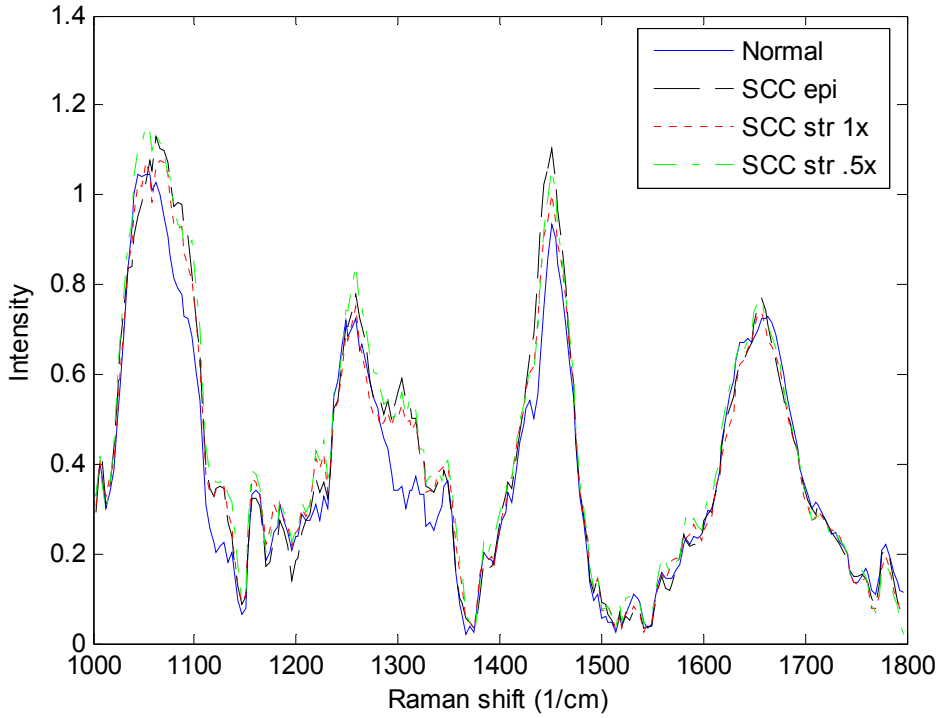


**Figure 2.4** Progression of Raman spectra obtained from rafts at (A) 10, (B) 15, and (C) 20 days in a single experiment. For each line, n = 2 measurements from each of 4 rafts.

transfer to the air-liquid interface. Each line represents the average spectrum from two measurements each on four samples of each kind of raft. Focusing on the same spectral region as before, at days 10 and 15, there is little difference between normal rafts and rafts with SCC cells in the stroma, but there is a significant difference ($p < .01$) between rafts with SCC cells in the epidermis and all other rafts. There are differences in other spectral regions, but 1300 to 1330 $cm^{-1}$ shows the most. At day 20, however, all rafts with dysplastic cells in any location gave equivalent Raman spectral signatures that were significantly different ($p < .001$) from those of normal rafts in the 1300 to 1330 $cm^{-1}$ range, and in the shoulder regions from about 1070 to 1100 $cm^{-1}$ and 1110 to 1130 $cm^{-1}$.

Since Raman spectra obtained at day 20 tended to show the most distinction between normal and all dysplastic rafts, measurements from day 20 of three different sets of experiments were combined to produce Figure 2.5 below. Each plot now represents

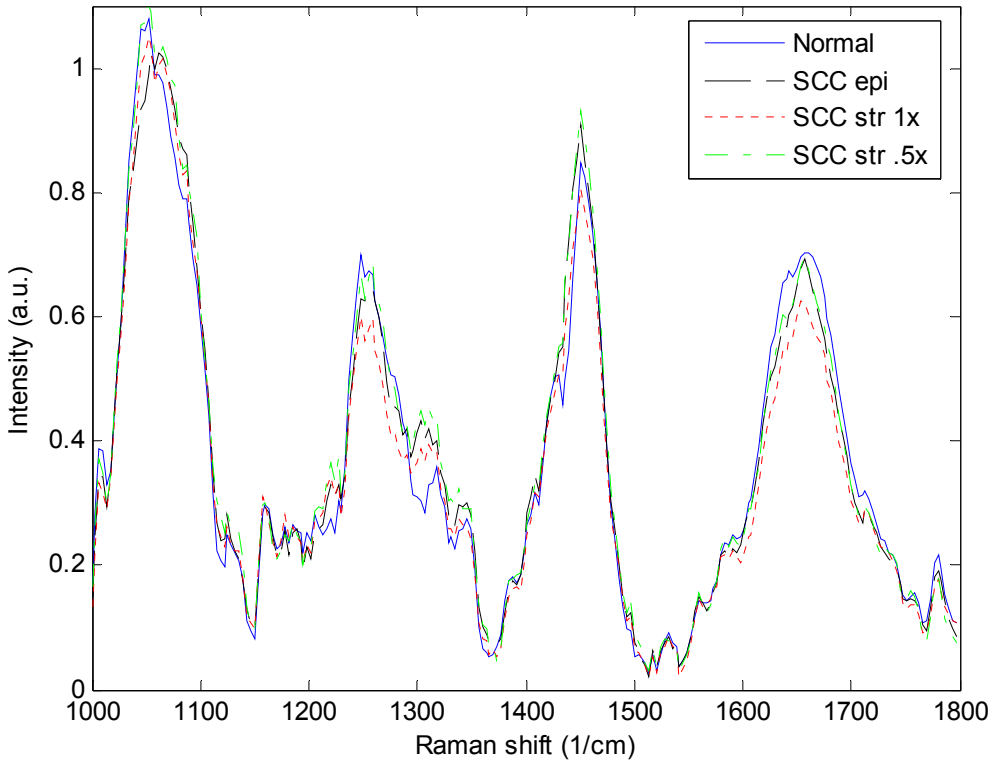


**Figure 2.5** Mean Raman spectra taken on day 20 of rafts from three sets of experiments. For each line, n = 2 measurements from each of 12 rafts.

the mean of two measurements from each of 12 rafts. Fewer wavenumbers show significant differences in this figure, but given the increase in sample size, the region from 1300 to 1320 $cm^{-1}$ still shows a significant difference ($p < .01$) between the normal rafts and any type of cancerous raft, while all dysplastic rafts are statistically equivalent.

Raman spectra from the epidermal layer only, taken on day 20, were also averaged over three sets of experiments and are shown in Figure 2.6. Since some rafts

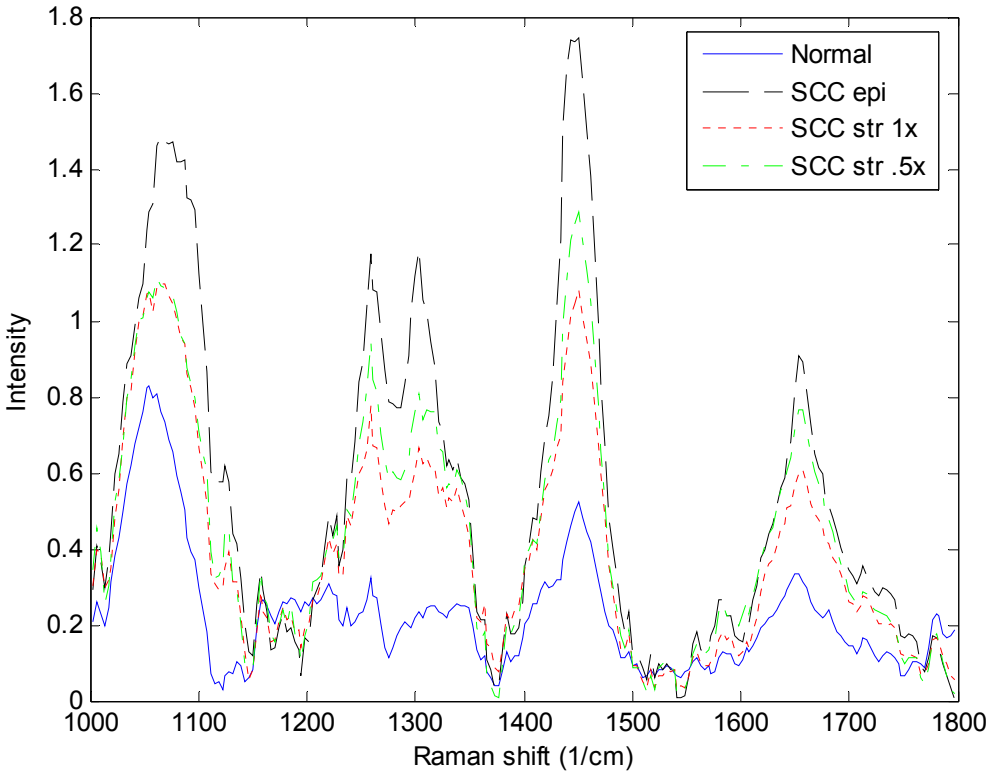


**Figure 2.6** Mean Raman spectra of epidermis only, taken on day 20, of rafts from three sets of experiments. For each line, n = 2 measurements from each of 8 rafts.

were saved intact for histology, each plot represents the mean of two measurements on each of eight raft epidermal layers that had been separated from the underlying stroma. This figure appears somewhat unusual at first, especially with regard to intensity differences, but all spectra were normalized over their entire range, which includes portions not shown in the figure. Considering the spectra as displayed produces significant differences across most of the wavenumbers between normal rafts and those with SCC cells in any location, while the epidermal layers of the rafts with SCC cells only in their stroma were mostly equivalent to one another but different from the other two types. If only this portion of the spectra were re-normalized to eliminate intensity differences (not shown), we find that epidermal Raman signatures from normal rafts are

still significantly different ($p < .01$) from all other raft types, and now the epidermal signatures from rafts with SCC cells originally in the stroma only or in the epidermis only are mostly equivalent, including in the 1300 to 1330 $cm^{-1}$ region. These findings can be seen simply by eye-balling the general line shapes while ignoring intensity differences in Figure 2.6 as well – the epidermal signatures from the three dysplastic rafts all appear to be quite similar to each other but different from the normal one.

The relationships among the mean Raman signatures of the epidermal and stromal layers of the same set of rafts are shown in more detail in Figure 2.7 below. Representative histological images of the different kinds of rafts are shown in Figure 2.8 as well. From Figure 2.7(A and B), we see that the stromal signatures of normal rafts and rafts with SCC cells only in the epidermis appear to be nearly identical, and these layers look very similar under standard histology in Figure 2.8(A and B). The stromal signatures of the two types of rafts with SCC cells only in the dermis, as seen in Figure 2.7(C and D), are also nearly identical, as were their histological findings, so only one example is shown in Figure 2.8(C). The stromal signatures of rafts with normal dermis layers were significantly different ($p < .01$), though, compared with the stromal signatures of the rafts with cancerous dermis layers, as expected. As seen when comparing the top row of Figure 2.7 to the bottom row, this difference is again primarily in the region of 1300 to 1320 $cm^{-1}$.

Figure 2.7 supports the idea reported in our earlier study[39] that much of the spectral variation in intact raft cultures derives from the epidermal layer, since there are much greater differences in the epidermal signatures among the different kinds of rafts compared with the stromal signatures. Figure 2.8 brings up an interesting point about the

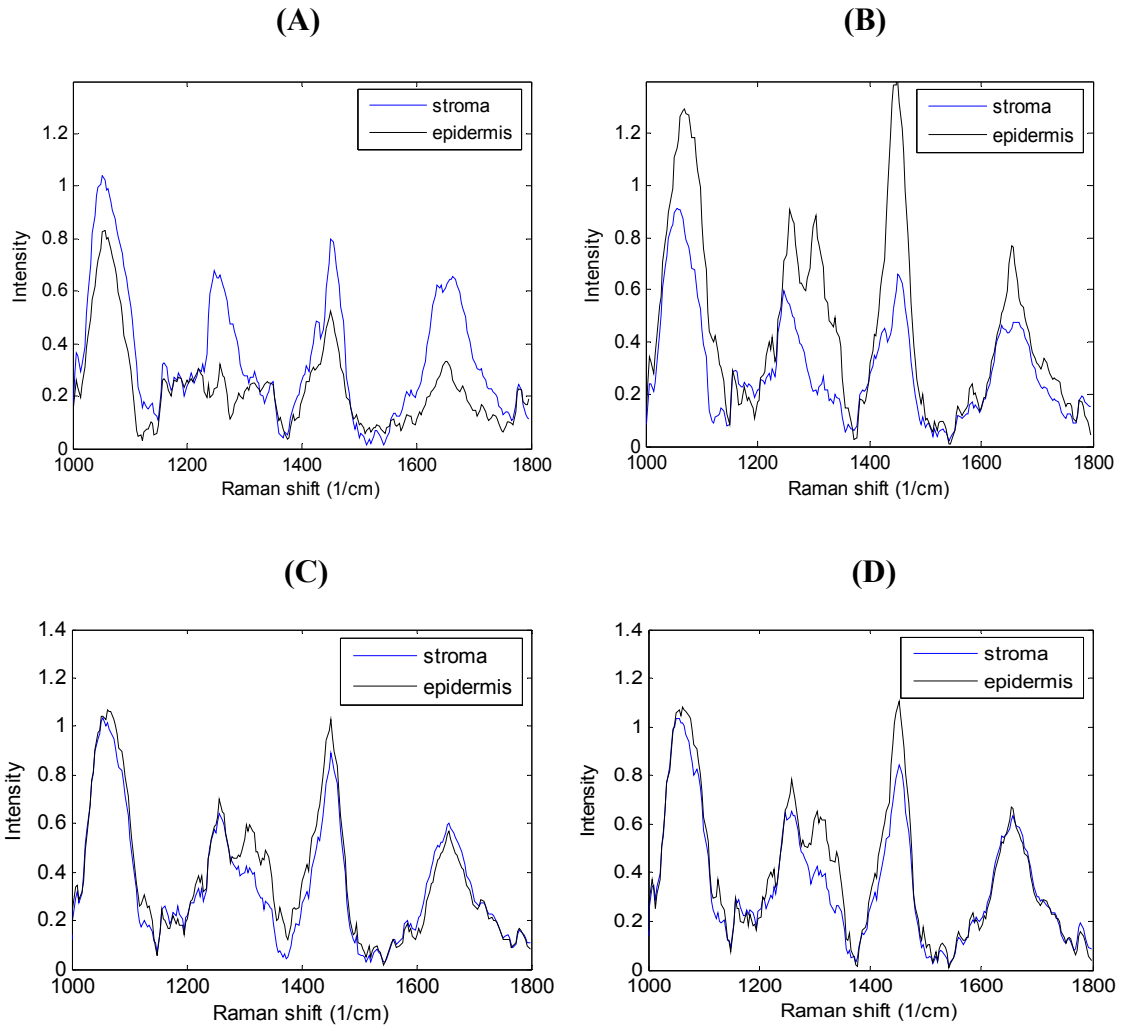


**Figure 2.7** Mean Raman spectra over same three sets of experiments, taken at day 20, comparing stromal and epidermal signatures of (A) normal, (B) SCC epi, (C) SCC str 1x, and (D) SCC str .5x rafts.

spectral variations of the epidermal layers seen in Figures 2.6 and 2.7. The epidermis of 2.8(C) does not visually look like the epidermis of 2.8(B), but spectrally, they are nearly equivalent. The pockets of SCC cells in the dermis of 2.8(C) do closely resemble the dysplastic epidermis of 2.8(B). The epidermis of 2.8(C) looks similar to, but not exactly like the normal one in 2.8(A), which is due at least in part to difficulties processing raft cultures for histology without damaging them, but they are spectrally distinct.

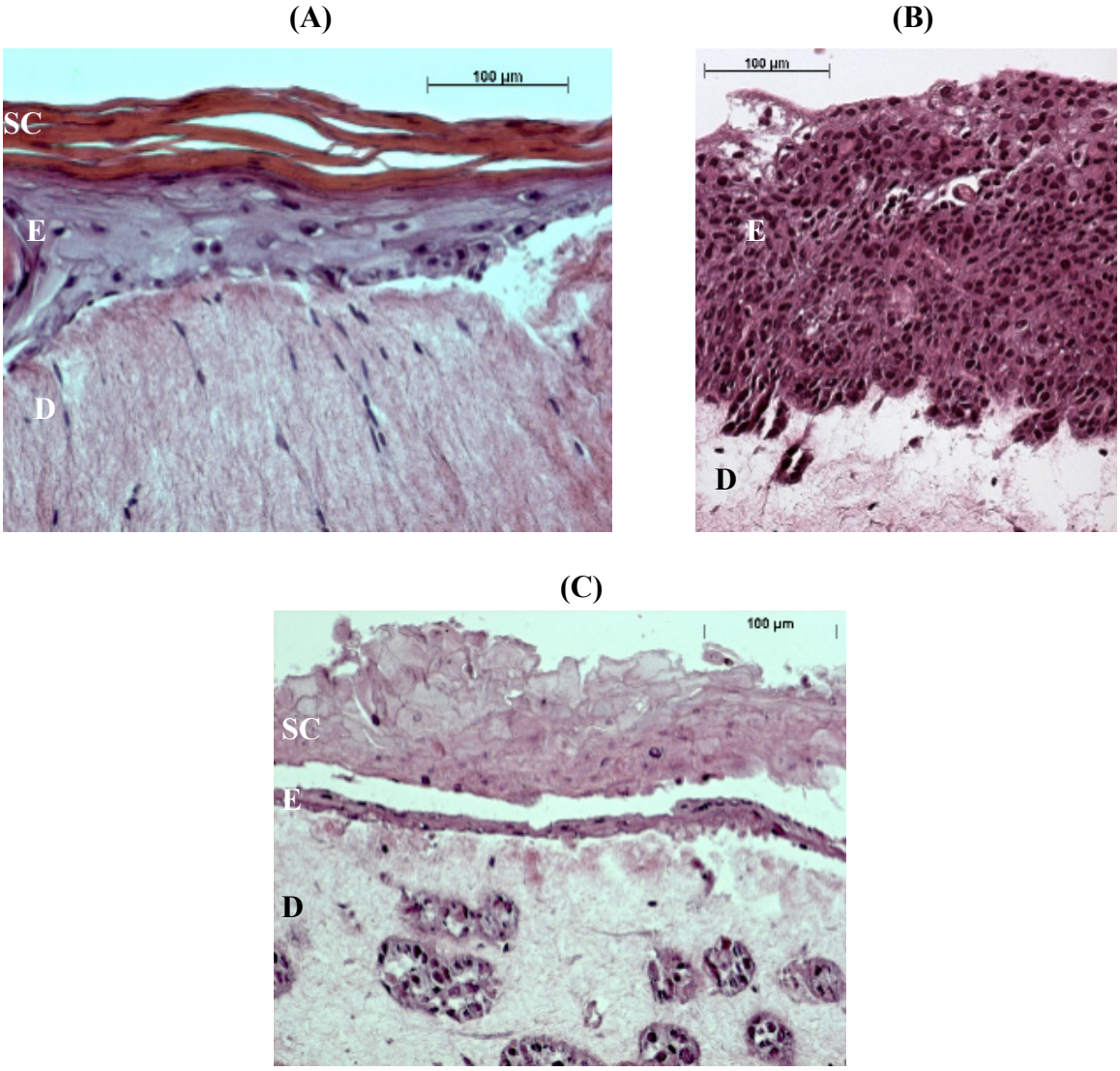


**Figure 2.8** Representative histological images of (A) normal raft, (B) raft with SCC cells in epidermis and normal stroma, and (C) raft with SCC cells in stroma and initially normal epidermis. SC, stratum corneum; E, other epidermis; D, dermis (stroma)

## Discussion

The results of this study agree fairly well with what was expected. The results seen in Figures 2.2 and 2.3 first demonstrated that when gathering Raman spectra with a macroscopic probe able to penetrate several hundred microns, the location of the cancerous cells does not significantly impact the signatures. Visually, figure 2.2 hinted at

a dose-dependant effect, but further studies and statistical analysis have indicated that, at least within the ranges used, concentration of SCC cells in the dermis is not a major factor in determining the Raman spectral shape. The same spectral region, approximately 1300 to 1330 $cm^{-1}$, showed the greatest differences between normal and dysplastic rafts both in our previous study[39] and in this study. The peaks in this spectral region can be attributed to a variety of molecules – lipids, proteins (amide III band), and DNA nucleotide bases. All of these molecules would be expected to be present in higher concentrations in cancerous vs. normal tissue, especially DNA, thus explaining the increase in Raman intensities in that region. The peak around 1450 $cm^{-1}$ can sometimes be useful for tissue discrimination as well, as in Figure 2.3, as it gives information about the relative contents of lipid and protein.

As demonstrated in Figure 2.4, the best results for distinguishing diseased from normal tissue seemed to be measurements taken at 20 days following the transfer of the rafts to the air-liquid interface. Rafts need about two weeks to fully develop, so this time frame seems reasonable for the maturation of keratinocytes and progression of SCC cells. Differentiated keratinocytes in the body tend to undergo apoptosis after about three weeks, which may explain why no useful data was able to be obtained past 20 days. SCC cells deposited in the stroma showed an interesting pattern of growth. Although we do not have histology exactly corresponding to the spectra in Figure 2.4, other experiments showed that the SCC cells were initially spread out fairly evenly with the fibroblasts, then began to gather in bunches as depicted in Figure 2.8(C), increase in number, and actually move toward the top of the dermis to some extent. This progression of events could certainly be the mechanism behind the spectral changes going from (A) to (C) in Figure

2.4. These results were also some of the first to demonstrate that Raman spectra obtained side-by-side from rafts with SCC cells seeded in either the epidermis or the dermis were equivalent, rather than relying on comparing these results to older ones.

The importance of Figure 2.5 is that we can still distinguish between normal and dysplastic rafts of any type when data from three different experiments are combined, using the same spectral region as before. Although there will always be slight inconsistencies between different batches of raft cultures, these results indicate that their construction, even with introducing SCC cells into the dermis, is fairly reproducible. This figure also indicates that this simple t-test at every wavenumber may not be appropriate for looking at larger amounts of data in cases where inherent variability masks out significant differences within individual time points.

As mentioned, Figures 2.6 and 2.7 can be interpreted in multiple ways. The Raman spectra from separated stroma layers are all fairly similar, though the rafts with SCC cells in the stroma do show an increase in the intensity of the 1307 $cm^{-1}$ DNA shoulder off of the 1270 $cm^{-1}$ peak, primarily due to collagen, relative to rafts with normal stroma. It is fairly easy to visualize how the combinations of epidermis and dermis signal from each part of 2.7 would combine to form the spectra seen in 2.4(C). One might expect greater differences in the stroma signatures, though perhaps signal from malignant cells deeper in the tissue is not collected as efficiently, or maybe it is an issue of beam geometry in not having the highly scattering epidermis above it to effectively spread out the photons and detect more cancerous cells.

The differences in spectral signatures from the epidermis layers only are more dramatic. Whether or not one believes that the observed general intensity differences are

a real effect, it is hard to argue with the line shapes, especially upon re-normalization, given that these results were seen in three different sets of experiments. The equivalence of epidermal spectra from rafts with SCC cells initially in just the epidermis or just the stroma, along with their nonequivalence with epidermal spectra from normal rafts, backs up our previous *in vivo* skin study and again suggests the ability of Raman spectroscopy to detect malignancy associated changes in a tissue prior to it actually becoming cancerous. Figure 2.8(C) shows that the epidermis of the "SCC stroma" raft clearly does not visually resemble that of the "SCC epi" raft in 2.8(B), but does more closely resemble the epidermis of the normal raft in 2.8(A). Unfortunately, raft cultures are notoriously difficult materials to process for histology, which has prevented our obtaining better pictures of rafts with SCC cells in the stroma to help either prove or disprove our case. It certainly appears, though, that when the SCC cells are seeded in the stroma, they produce some sort of biochemical signal that both draws them together in clusters and influences the epidermal cells above them to undergo changes that are detectable with Raman spectroscopy, but not with a standard histology preparation. The development of these signals is another possible explanation for the time course seen in Figure 2.4.

Several points still need to be addressed with this study. Raft cultures are good models of skin, both structurally and spectroscopically, but they are not perfect. There are no blood vessels or inflammatory cells in the dermis, and there is no basement membrane between the epidermis and dermis. The latter fact may be relevant in this case not only because of a missing component that may contribute to *in vivo* Raman, but also because its presence may affect the transmission of any biochemical signals between the dermis and epidermis. More consistency still needs to be achieved between different

batches of rafts as well. Instrumentation issues have prevented the gathering of useful depth-resolved data on intact rafts, which would be a solid piece of supporting evidence for these findings and for the *in vivo* skin findings.

In conclusion, we have demonstrated the ability to use Raman spectroscopy to distinguish between normal and dysplastic raft cultures regardless of where the SCC cells are located, and that the presence of disease in the stroma can be detected in the epidermis. The signals obtained from the rafts with the macroscopic probe system are fairly well understood, but more study with confocal Raman spectroscopy and better histology is required to truly understand the depth-dependent basis of the signals. Although these raft cultures are not perfect models of skin or skin cancer, they have been shown to provide valuable information that will be useful for the concurrent *in vivo* studies on diagnosing nonmelanoma skin cancers.

**References**


1. American Cancer Society. www.cancer.org. (2005).

2. Freedberg I *et. al., eds.* Fitzpatrick's Dermatology in General Medicine, 6th edn. (McGraw Hill: 2003).

3. Caspers, P.J., Lucassen, G.W., Wolthuis, R., Bruining, H.A. & Puppels, G.J. In vitro and in vivo Raman spectroscopy of human skin. *Biospectroscopy* **4**, S31-39 (1998).

4. Caspers, P.J., Lucassen, G.W., Carter, E.A., Bruining, H.A. & Puppels, G.J. In vivo confocal Raman microspectroscopy of the skin: noninvasive determination of molecular concentration profiles. *J Invest Dermatol* **116**, 434-442 (2001).

5. Caspers, P.J., Lucassen, G.W. & Puppels, G.J. Combined in vivo confocal Raman spectroscopy and confocal microscopy of human skin. *Biophys J* **85**, 572-580 (2003).

6. Gniadecka, M., Faurskov Nielsen, O., Christensen, D.H. & Wulf, H.C. Structure of water, proteins, and lipids in intact human skin, hair, and nail. *J Invest Dermatol* **110**, 393-398 (1998).

7. Chrit, L. et al. In vivo chemical investigation of human skin using a confocal Raman fiber optic microprobe. *J Biomed Opt* **10**, 44007 (2005).

8. Osada, M., Gniadecka, M. & Wulf, H.C. Near-infrared Fourier transform Raman spectroscopic analysis of proteins, water and lipids in intact normal stratum corneum and psoriasis scales. *Exp Dermatol* **13**, 391-395 (2004).

9. Huang, Z. et al. Raman spectroscopy of in vivo cutaneous melanin. *J Biomed Opt* **9**, 1198-1205 (2004).

10. Eikje, N.S., Ozaki, Y., Aizawa, K. & Arase, S. Fiber optic near-infrared Raman spectroscopy for clinical noninvasive determination of water content in diseased skin and assessment of cutaneous edema. *J Biomed Opt* **10**, 14013 (2005).

11. L. Knudsen, C.K.J., P. A. Philipsen, M. Gniadecka, H. C. Wulf, Natural variations and reproducibility of in vivo near-infrared Fourier transform Raman spectroscopy of normal human skin. *Journal of Raman Spectroscopy* **33**, 574-579 (2002).

12. Ermakov, I.V., Sharifzadeh, M., Ermakova, M. & Gellermann, W. Resonance Raman detection of carotenoid antioxidants in living human tissue. *J Biomed Opt* **10**, 064028 (2005).

13. Hata, T.R. et al. Non-invasive raman spectroscopic detection of carotenoids in human skin. *J Invest Dermatol* **115**, 441-448 (2000).

14. Ermakov, I.V., Ermakova, M.R., Gellermann, W. & Lademann, J. Noninvasive selective detection of lycopene and beta-carotene in human skin using Raman spectroscopy. *J Biomed Opt* **9**, 332-338 (2004).

15. Percot, A. & Lafleur, M. Direct observation of domains in model stratum corneum lipid mixtures by Raman microspectroscopy. *Biophys J* **81**, 2144-2153 (2001).

16. Neubert, R., Rettig, W., Wartewig, S., Wegener, M. & Wienhold, A. Structure of stratum corneum lipids characterized by FT-Raman spectroscopy and DSC. II. Mixtures of ceramides and saturated fatty acids. *Chem Phys Lipids* **89**, 3-14 (1997).

17. Edwards, H.G.M., A.C. Williams, and B.W. Barry Potential applications of FT-Raman spectroscopy for dermatological diagnostics. *J Molec Struct* **347**, 379-388 (1995).

18. Wohlrab, J., Vollmann, A., Wartewig, S., Marsch, W.C. & Neubert, R. Noninvasive characterization of human stratum corneum of undiseased skin of patients with atopic dermatitis and psoriasis as studied by Fourier transform Raman spectroscopy. *Biopolymers* **62**, 141-146 (2001).

19. M. Gniadecka, H.C.W., N. Nymark Mortensen, O. Faurskov Nielsen, D. H. Christensen, Diagnosis of Basal Cell Carcinoma by Raman Spectroscopy. *Journal of Raman Spectroscopy* **28**, 125-129 (1997).

20. Nijssen, A. et al. Discriminating basal cell carcinoma from its surrounding tissue by Raman spectroscopy. *J Invest Dermatol* **119**, 64-69 (2002).

21. Choi, J. et al. Direct observation of spectral differences between normal and basal cell carcinoma (BCC) tissues using confocal Raman microscopy. *Biopolymers* **77**, 264-272 (2005).

22. Sigurdsson, S. et al. Detection of skin cancer by classification of Raman spectra. *IEEE Trans Biomed Eng* **51**, 1784-1793 (2004).

23. Gniadecka, M. et al. Melanoma diagnosis by Raman spectroscopy and neural networks: structure alterations in proteins and lipids in intact cancer tissue. *J Invest Dermatol* **122**, 443-449 (2004).

24. Lieber, C.A., Ellis, D., Billheimer, D., Mahadevan-Jansen, A. In vivo confocal Raman spectroscopy of skin nonmelanomas. *submitted* (2005).

25. Nieburgs, H.E. Recent progress in the interpretation of malignancy associated changes (MAC). *Acta Cytol* **12**, 445-453 (1968).

26. Nieburgs, H.E., Herman, B. E., and Reisman, H. Buccal cell changes in patients with malignant tumors. *Lab Invest* **2**, 80-88 (1962).

27. Nieburgs, H.E. et al. Malignancy associated changes (MAC) in blood and bone marrow cells of patients with malignant tumors. *Acta Cytol* **11**, 415-423 (1967).

28. Us-Krasovec, M. et al. Malignancy associated changes in epithelial cells of buccal mucosa: a potential cancer detection test. *Anal Quant Cytol Histol* **27**, 254-262 (2005).

29. Sacile, R.M., E. Ruggiero, C. Nieburgs, H.E. Nicolo, G. A decision support system to detect morphologic changes of chromatin arrangement in normal-appearing cells. *IEEE Trans NanoBioscience* **2**, 118-123 (2003).

30. Ikeda, N. et al. Malignancy associated changes in bronchial epithelial cells and clinical application as a biomarker. *Lung Cancer* **19**, 161-166 (1998).

31. Guillaud, M. et al. Exploratory analysis of quantitative histopathology of cervical intraepithelial neoplasia: objectivity, reproducibility, malignancy-associated changes, and human papillomavirus. *Cytometry A* **60**, 81-89 (2004).

32. Kemp, R.A., MacAulay, C., Garner, D. & Palcic, B. Detection of malignancy associated changes in cervical cell nuclei using feed-forward neural networks. *Anal Cell Pathol* **14**, 31-40 (1997).

33. Kasper, H.U., Haroske, G., Geissler, U., Meyer, W. & Kunze, K.D. Diagnostic and prognostic relevance of malignancy-associated changes in cervical smears. *Anal Quant Cytol Histol* **19**, 482-488 (1997).

34. Anderson, N. et al. Malignancy-associated changes in lactiferous duct epithelium. *Anal Quant Cytol Histol* **25**, 63-72 (2003).

35. Boroday, N., Klyushin, D., Petunin, Y. & Andrushkiw, R. Analysis of malignancy-associated DNA changes in interphase nuclei of buccal epithelium in persons with breast diseases. *Exp Oncol* **26**, 158-160 (2004).

36. Mommers, E.C., Poulin, N., Meijer, C.J., Baak, J.P. & van Diest, P.J. Malignancy-associated changes in breast tissue detected by image cytometry. *Anal Cell Pathol* **20**, 187-195 (2000).

37. Roy, H.K. et al. Four-dimensional elastic light-scattering fingerprints as preneoplastic markers in the rat model of colon carcinogenesis. *Gastroenterology* **126**, 1071-1081; discussion 1948 (2004).

38. Roy, H.K. et al. Risk stratification of colon carcinogenesis through enhanced backscattering spectroscopy analysis of the uninvolved colonic mucosa. *Clin Cancer Res* **12**, 961-968 (2006).

39. Viehoever, A.R., Anderson, D., Jansen, D. & Mahadevan-Jansen, A. Organotypic raft cultures as an effective in vitro tool for understanding Raman spectral analysis of tissue. *Photochem Photobiol* **78**, 517-524 (2003).

# CHAPTER IV

# SUMMARY AND RECOMMENDATIONS

## Summary

I set out my objectives and specific aims in a brief first chapter, and the second chapter presented a wealth of background information on skin cancer and on the principles and uses of optical spectroscopy, primarily Raman. In the manuscript, we have demonstrated that Raman spectroscopy can distinguish between normal and dysplastic raft cultures regardless of where the SCC cells are located and their seeding densities. We showed that the presence of disease in the stroma can be detected in the epidermis, even when the epidermis still looks normal with standard histology. These findings support our earlier *in vivo* skin study and offer additional evidence for the ability of spectroscopy to detect pre-malignant changes.

## Recommendations for future work

Several points still need to be addressed with this study. Raft cultures are good models of skin, but they are not perfect. There are no blood vessels or inflammatory cells in the dermis, and there is no basement membrane between the epidermis and dermis. Improving the raft model by introducing more components may provide better spectral characteristics, though it may not be worth the added complexity. More consistency still needs to be achieved between different batches of rafts as well. Instrumentation and other issues have prevented the gathering of useful depth-resolved data on intact rafts,

which would be a solid piece of supporting evidence for these findings and for the *in vivo* skin findings. Better methods to ensure quality histological images of raft cultures would provide a benefit to this study as well.